Large-Scale Stationary and Turbulent Flow over Topography

GEOFFREY K. VALLIS AND JOHN O. ROADS

Scripps Institution of Oceanography, University of California, San Diego, La Jolla, CA 92093

(Manuscript received 20 March 1984, in final form 27 August 1984)

ABSTRACT

Time averaged fields produced by a two-level, quasi-geostrophic, nonlinear time-dependent model of large-scale flow over topography are compared to results from stationary linear theory in order to assess the influence of transient eddies. It is shown that stationary linear theory predicts excessive amplitudes and has a low phase correlation with these time-averaged fields. Addition of the stationary nonlinear terms gives only a slight improvement. The transient eddy fluxes are responsible for reducing the amplitude of the linear solutions. Resonant effects evident in the linear models are highly damped, but still noticeable, in the turbulent solutions. The energetics of the stationary flow show that the transfer of stationary to transient energy is significant. Instability analyses of the time-averaged flow suggest that unstable perturbations are likely to arise which have structures qualitatively similar to time-averaged variance fields. We conclude that the time averages in such turbulent models depend both upon the stationary forcings and the instabilities that arise and that neglect of transient fluxes will lead to unrealistic results.

1. Introduction

The simplest models used to describe stationary eddies are the stationary linear models linearized around a zonal state (e.g., Saltzman, 1968). The primary justification for these models comes from the observation that the stationary eddies are very much weaker than the zonal flow—the eddy stationary energy is an order of magnitude smaller than the zonal stationary energy (Holopainen, 1970).

The effect of the transient eddies has often been regarded as implicit through their effect on the zonal flow and intermediate to small scales. Indeed, many linear models do produce stationary anomalies in qualitative agreement with some observations (e.g., Alpert *et al.*, 1983). However, some observational studies suggest that the transient eddies (which have more energy than the stationary eddies) have an important influence on the actual stationary eddies (e.g., Holopainen *et al.*, 1982) and especially on those produced by linear models (e.g., Youngblut and Sasamori, 1980; Opsteegh and Vernekar, 1982). Other evidence lies in the instability properties associated with the stationary eddies. If these eddies are unstable then they are likely to give rise to perturbations that may draw energy from the stationary flow in an organized manner, eventually leading to a different time averaged field. A number of simple models of this interaction have been proposed (e.g., Frederiksen, 1978; Lin, 1980; Sasamori and Youngblut, 1981).

The direct effect of the transients on the stationary eddies has received little attention, partly because it is very difficult, in the real atmosphere, to isolate their effects. They will affect the stationary flow by direct energy transfer and by stochastic perturbations. How important these processes are, which are neglected in linear models, and, concomitantly, how realistic the results from such models are, is not well understood.

One step toward understanding such problems is to rigorously compare linear theory with the time averages in a nonlinear time-dependent model (e.g., Roads, 1981; Phillips, 1982). The linear model can be identical with the full model in all respects other than the omission of nonlinearities. In particular it can use the same stationary forcings and finite differencing of the turbulent model. Further, the linear model can use the time-averaged state of the turbulent model. By comparing the time-averaged (stationary) response of the turbulent model with the linear model, linearized around the mean zonal flow of the full model, the effects of the transient eddies can be isolated.

In this paper we report the results of such a study with a turbulent (i.e., time dependent, highly nonlinear) two-level quasi-geostrophic model on a beta plane with specified topography. The turbulent model (often denoted the "full" model below) is compared to the response in various abridged models—a purely linear model, a linear model with nonlinear stationary fluxes included as nonhomogeneous forcing terms, and linear models with nonlinear and transient thermodynamic or vorticity fluxes similarly included. Aside from the omission of one or more of the above processes, the models are identical. Energetics of the models are decomposed into stationary and transient

components to examine the energy flow. Finally the stability of the solutions is examined. Here the aim is to see whether the variance of the full model is related to the unstable eigensolutions of the time-averaged flow.

The two-level model should not be regarded as quantitatively "realistic", its primary weakness for these studies being the imposition of a rigid lid at the top of the model atmosphere which may prevent energy in the stationary waves from propagating upward. This might enhance any resonance characteristics in the models (e.g., Smagorinsky, 1953). However, as shown, for example, by Tung and Lindzen (1980) tropospheric resonance is possible in atmospheric models which incorporate realistic zonal wind shears.

Overall, we are interested in how stationary topography is related to the time-averaged fields in the turbulent model, in the hope of ultimately understanding the time-averaged response through the use of simple models, in which turbulent processes are parameterized. For example, White and Green (1982) found that the asymmetric eddies as well as the zonal flow must include parameterizations for the transient eddies.

The basic model is described in Section 2. A description of the simulations and their energy budgets can be found in Section 3. Section 4 contains a comparison with linear theory. Section 5 is a description of the instability analysis. Section 6 contains the summary and conclusions.

2. Model

The two-level, beta-plane, quasi-geostrophic channel model comprises upper and lower level vorticity equations, a thermodynamic equation and boundary conditions. These equations may be written, in standard notation, as

$$\frac{\partial}{\partial t}\nabla^2\psi_1 + J(\psi_1, \nabla^2\psi_1 + \beta y) = f\frac{\omega}{\Delta p} - D_1, \quad (1)$$

$$\frac{\partial}{\partial t}\nabla^2\psi_3 + J(\psi_3, \nabla^2\psi_3 + \beta y) = -f\frac{\omega}{\Delta p} + f\frac{\omega_s}{\Delta p} - D_3, \quad (2)$$

$$\lambda^2\frac{\partial \tau}{\partial t} + \lambda^2 J(\psi, \tau) = \lambda^2 F_\tau + \frac{f\omega}{2\Delta p}. \quad (3)$$

The vertical pressure velocity is zero at the upper boundary and at the surface, ω_s, is given by

$$\frac{f\omega_s}{\Delta p} = -\frac{\rho_s g f}{\Delta p}J(\omega_3, h') - K'f^2\frac{\rho_s}{\Delta p}\nabla^2\psi_3 = -J(\psi_3, h) - K\nabla^2\psi_3, \quad (4)$$

where ψ_1 and ψ_3 are the upper and lower level streamfunctions; ψ and τ are the barotropic and thermal streamfunctions defined by $\psi = (\psi_1 + \psi_3)/2$, $\tau = (\psi_1 - \psi_3)/2$; h' is the dimensional orographic height and F_τ is the thermodynamic forcing. The flow is governed by these parameters as well as the value of β, the meridional derivative of the coriolis parameter; the inverse deformation radius λ, which is a measure of the static stability; the surface friction coefficient K; and the dimensions of the domain (zonal extent, L_x, 16 000 km and meridional extent, L_y, 8000 km). In (1) and (2) D_1 and D_3 are high-order diffusion operators designed to remove enstrophy and keep the energy spectra smooth at high wavenumbers. They have a negligible effect on low wavenumbers and are parameterized by $D_i = \nu\nabla^6\psi_i$. The numerical values of some of the parameters are

$\beta = 1.5 \times 10^{-11}$ s^{-1} m^{-1}
$\Delta p = 400$ mb
$\lambda^2 = 3.16 \times 10^{-12}$ m^{-2} (corresponding to a nondimensional wavenumber 4.5)
$\nu = 1.4 \times 10^{16}$ m^4 s^{-1}
$K = (1/2.9)$ days^{-1}.

By eliminating the vertical velocity the equations may be combined into equations representing the conservation of potential vorticity at the upper and lower levels,

$$\frac{\partial}{\partial t}q_1 + J(\psi_1, q_1) = -2\lambda^2 F_\tau - D_1, \quad (5)$$

$$\frac{\partial}{\partial t}q_2 + J(\psi_3, q_3) = +2\lambda^2 F_\tau - D_3, \quad (6)$$

where

$$\left.\begin{aligned} q_1 &= \nabla^2\psi_1 + \lambda^2(\psi_3 - \psi_1) + \beta y \\ q_3 &= \nabla^2\psi_3 + \lambda^2(\psi_1 - \psi_3) + \beta y + h \\ D_3 &= \nu\nabla^6\psi_3 + K\nabla^2\psi_3 \\ D_1 &= \nu\nabla^6\psi_1 \end{aligned}\right\}.$$

The vertical velocity is obtained from an omega equation.

The channel is periodic in the x-direction and has zero flow through the boundaries along the northern and southern edges. A no-slip condition is also imposed on the zonally averaged zonal wind. An appropriate spectral expansion of the streamfunction is then

$$\psi(x, y, t) = \sum_{l=1}^{N-1} b_{0l}(t)\cos ly + \sum_{l=1}^{N-1}\sum_{\substack{k=-(N-1)\\k\neq 0}}^{k=N-1} b_{kl}(t)\sin ly e^{ikz}. \quad (7)$$

Here x and y are nondimensional coordinates defined by $x = x^*2\pi/L_x$; $y = y^*\pi/L_y$, where the asterisk denotes a dimensional variable. Note that no eddy activity is allowed on the boundary and a temperature gradient can exist across the domain.

Evaluation of the nonlinear Jacobian terms is not trivial if energy and enstrophy conservation are demanded. Essentially, terms not involving the zonal flow are evaluated exactly by Orszag's (1971) staggered grid algorithm—a spectral transform technique. Wave–mean flow terms make use of transform techniques and interaction coefficients (Vallis, 1985).

The form of the thermodynamic forcing is

$$F_\tau = \left(\frac{A_k}{2} + C\tau_k\right).$$

Here C gives a radiative damping, with a time scale of about 23 days (2×10^6 seconds). The zonal forcing component (A_{01}) is set to a value corresponding to 0.9 K day. In the absence of eddies this radiative forcing yields a symmetric radiative-equilibrium zonal wind of about 35 m s^{-1} at the upper level and an almost zero, but negative, lower level wind (Fig. 1). The lower level wind would be exactly zero but for the high-order diffusion operators (the enstrophy removers).

We note here that it is not our intention to perform a complete parameter study of the Eqs. (5) and (6). We propose only a study of the effects of a localized range of mountains and a localized heat source. To this end experiments (denoted M1, M2) were performed with a strip of mountains through the whole meridional extent of the domain, and of 2000 km zonal extent. The total height in the strip is 2 km (M2) or 4 km (M1). In experiments H2 and H1 a heat source replaces the mountains, with effective total heating rates of 4.5 K day^{-1} (H2) and 9 K day^{-1} (H1). The spectral amplitudes of the heating and orography are illustrated in Fig. 6. Note the spectral expansions show a zero at wavenumber 8. The parameter range of the forcings is similar to that of Kalnay-Rivas and Merkine (1981) and other idealized studies.

3. Numerical experiments

The full (i.e., time dependent, nonlinear) model was integrated for 120 days (after a warm-up period of 30 days) with mountains (M1 and M2), localized heating (H1 and H2) or neither (C1, the control); M1 and C1 were further integrated for 120 more days to give some measure of variance.

a. Physical space response

The time and zonally-averaged wind for the various experiments is illustrated in Fig. 1. Note that the shear is reduced by about a factor of two from the equilibrium value, and the surface wind has the typical easterly, westerly, easterly variation. Note in particular that the main features of the zonal wind are not altered by the inclusion of orography or asymmetric heating.

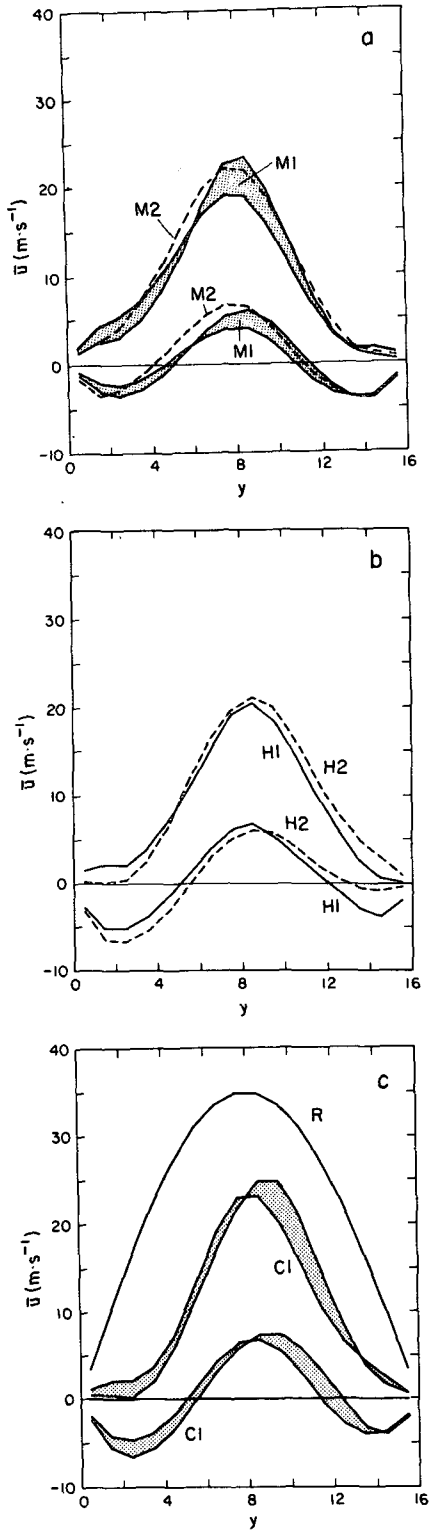

FIG. 1. Time- and zonally-averaged zonal winds at the upper and lower levels for (a) M1 and M2; (b) H1 and H2 and (c) C1. In (a) and (c) the shaded regions indicate two different 120-day integrations (M1a and M1b, and C1a and C2b), thereby giving some measure of the variability of the runs. In (c) the curve R is the radiative-equilibrium zonal wind.

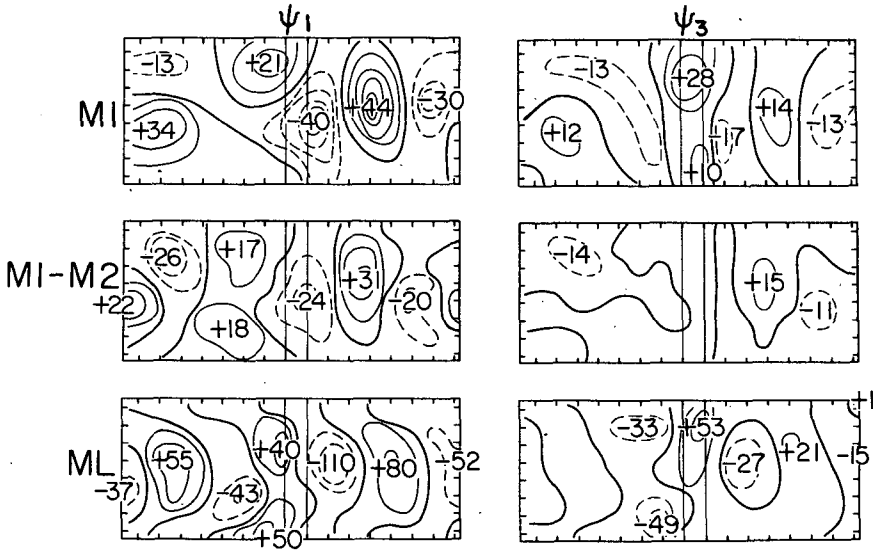

FIG. 2. Upper and lower level streamfunctions, for the mountain cases M1 and M2: (a) is the time averaged results from the full model for M1, (b) displays the difference field M1 − M2 and (c) shows the fields predicted by linear theory using the zonal wind of the full model for M1. Units are arbitrary with 10 units corresponding to a geopotential height of approximately 40 meters.

The streamfunctions, minus the zonal mean, are displayed in Figs. 2 and 3. The amplitudes are in nondimensional units with a value of 10 corresponding roughly to a geopotential height of 40 meters. The response has a wave train propagating about halfway round the domain downstream of the mountains, with a stationary high north and west of the mountains, and a low directly east. The anomaly flow pattern is shifted eastward somewhat at the lower level, and lowered in amplitude. The difference map (M1 − M2) shows some reduction in amplitude, and some slight phase shifts.

The nonlinearity inherent in the solutions is most noticeable by comparing the linear solution with the full solution (i.e., rows 3 and 1 of Figs. 2 and 3). The linear solution uses the time-averaged zonal wind from M1 and the same stationary topographic forcings. The amplitudes of the linear solution are about three times as large as the full solutions and have larger responses near the critical latitudes in the

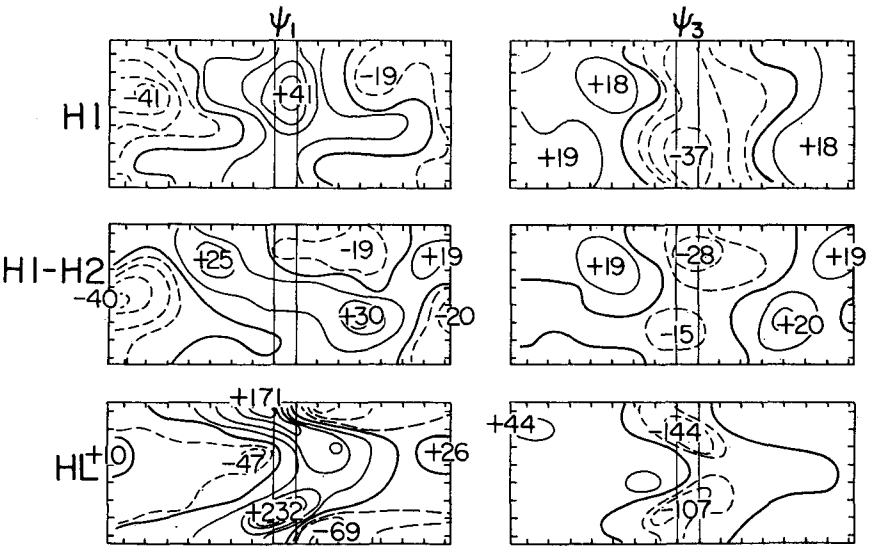

FIG. 3. As in Fig. 2 but for the heating cases H1 and H2.

heating cases. The comparison with linear theory is developed more fully in Section 4.

b. Energetics

The model energetics are decomposed spectrally into kinetic and available potential energy for both stationary and transient components. The unforced, inviscid model conserves energy exactly. The equations for the kinetic energy budget are obtained by taking the time average of (1) and (2) and multiplying by $-[\psi_{1\mathbf{k}}]$ and $-[\psi_{3\mathbf{k}}]$ and adding the resulting expressions. A square bracket denotes a time average, a prime a deviation therefrom and a subscript $\mathbf{k}$ the $\mathbf{k}$th spectral mode. The potential energy budget is similarly obtained from (3).

The budget equations for the stationary flow are, for each wavenumber $\mathbf{k}$,

$$\frac{1}{2}k^2\frac{d}{dt}([\psi_{\mathbf{k}}]^2 + [\tau_{\mathbf{k}}]^2 = T_{\mathbf{k}}([K],[K]) + T_{\mathbf{k}}([K],K') + C_{\mathbf{k}}([P],[K]) + S_{\mathbf{k}}([K]), \quad (8)$$

$$\lambda^2\frac{d}{dt}[\tau_{\mathbf{k}}]^2 = \mathrm{T}_{\mathbf{k}}([P],[P]) + T_{\mathbf{k}}([P],P') - C_{\mathbf{k}}([P],[K]) + S_{\mathbf{k}}([P]). \quad (9)$$

The left-hand sides of (4) and (5) are the total rates of change of the time averaged kinetic and potential energies. The terms on the right-hand side are, for each wavenumber $\mathbf{k}$.

$T([K],[K])$(transfer of stationary kinetic energy)

$$= \frac{1}{2}[\psi_1]J([\psi_1],[\nabla^2\psi_1]) + \frac{1}{2}[\psi_3]J([\psi_3],\nabla^2[\psi_3] + h),$$

$T([K],K')$(transfer of stationary to transient kinetic energy)

$$= \frac{1}{2}[\psi_1][J(\psi',\nabla^2\psi_1')] + \frac{1}{2}[\psi_3][J(\psi_3',\nabla^2\psi_3')],$$

$S([K])$(frictional sink of stationary kinetic energy)

$$= \frac{1}{2}[\psi_3][D_3] + \frac{1}{2}[\psi_1][D_1],$$

$C([P],[K])$(conversion of energy from potential to kinetic

$$= -\frac{f}{\Delta p}[\omega][\tau],$$

$T([P],[P])$(transfer of stationary potential energy)

$$= -2\lambda^2[\tau]J([\psi],[\tau]),$$

$T([P],P')$(transfer of stationary to transient potential energy)

$$= -2\lambda^2[\tau][J(\psi',\tau')],$$

$S([P])$(diabatic source of stationary potential energy)

$$= 2\lambda^2[\tau][F_\tau].$$

The transient energy budget is similar. For an overall view of the model energy cycle we decomposed the above balance equations into budgets for the zonally averaged flow and the remainder for both transient and stationary flow. These block energy diagrams are depicted in Figs. 4 and 5. The energy spectra are graphed in Fig. 6 and the budgets are graphed by zonal wavenumber in Figs. 7 and 8. (The energy in the stationary field in the control experiment, except for the zonal flow, is much smaller than that in the topographic cases, as can be seen from Fig. 6. The energy in the nonzonal flow is nonzero because the integration time is finite.)

The total energy spectra (Fig. 6) depends only slightly on the inclusion of topography, and in all cases the slope and magnitudes are entirely reasonable. One cannot ask for a k^{-3} spectra even for a model with $N = 16$, since such a spectra depends on very non-local interactions which are not simulated. Nor for that matter, should we expect such a spectra in the atmosphere since its quasi two-dimensionality breaks down too soon. (The spectral slope in this model is about 3.5.) The ratio of energy in the transient to the stationary flow generally increases

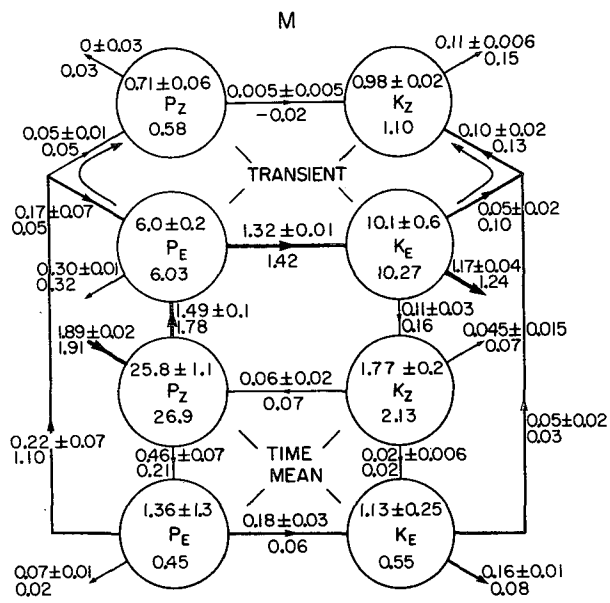

FIG. 4. Energy diagram for M1 and M2. The upper part of the figure shows the transient energy budget and the lower part of the figure the stationary energy budget. P denotes the available potential energy which is separated into zonal (subscript z) and eddy (subscript E) for both stationary and transient energy. K denotes kinetic energy and is separated similarly. The arrows denote the direction of the energy flow. Energies are in units of 10^5 J m^{-2} and the transfers are in W m^{-2}. The upper numbers (with estimated errors from two 120 day integrations) correspond to M1 and the lower numbers to M2.

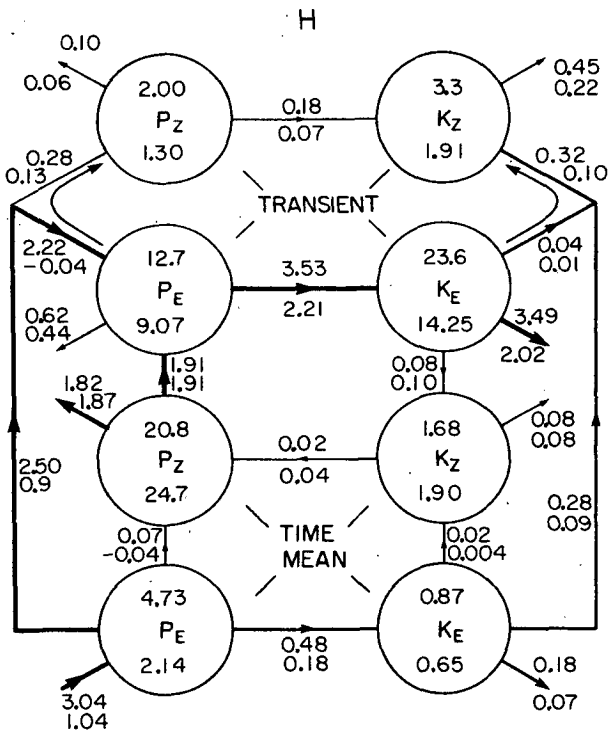

FIG. 5. As in Fig. 4 but for H1 and H2.

with wavenumber. At high wavenumbers, energy is almost all transient (as it is for the atmosphere, cf. Boer and Shepherd, 1983).

The total energy budgets for all cases (Fig. 7) are typical of quasi-geostrophic turbulence: potential energy is transferred by baroclinic instability of the mean flow to the waves mainly between wavenumbers 3 and 7. This is balanced by a (local) conversion to kinetic energy where it is transferred upscale to be ultimately dissipated by friction. The only significant difference between cases is the additional source of potential energy at low wavenumbers in the heating cases. There are only quantitative differences between H1 and H2, and M1 and M2; so only those for M1 and H1 are shown. The energy in the zonal flow (both stationary and total) is very similar for all experiments M1, M2, H1, H2 and C1. Its value is about 50% higher than that required for baroclinic instability (see Section 4c).

The maintenance of the stationary energies for M1 is illustrated overall in Fig. 4 and as a function of wavenumber in Fig. 8. The level of stationary energy in M1 is generally realistic, even though the zonal shear is highly supercritical. The zonal baroclinicity is actually slightly lower than that in the real atmosphere. If the baroclinicity were raised (by raising the zonal forcing), the instability and turbulence activity would be stronger, and the eddies would probably be more efficient at extracting energy from the stationary flow. Note the general direction of the energy cycle:

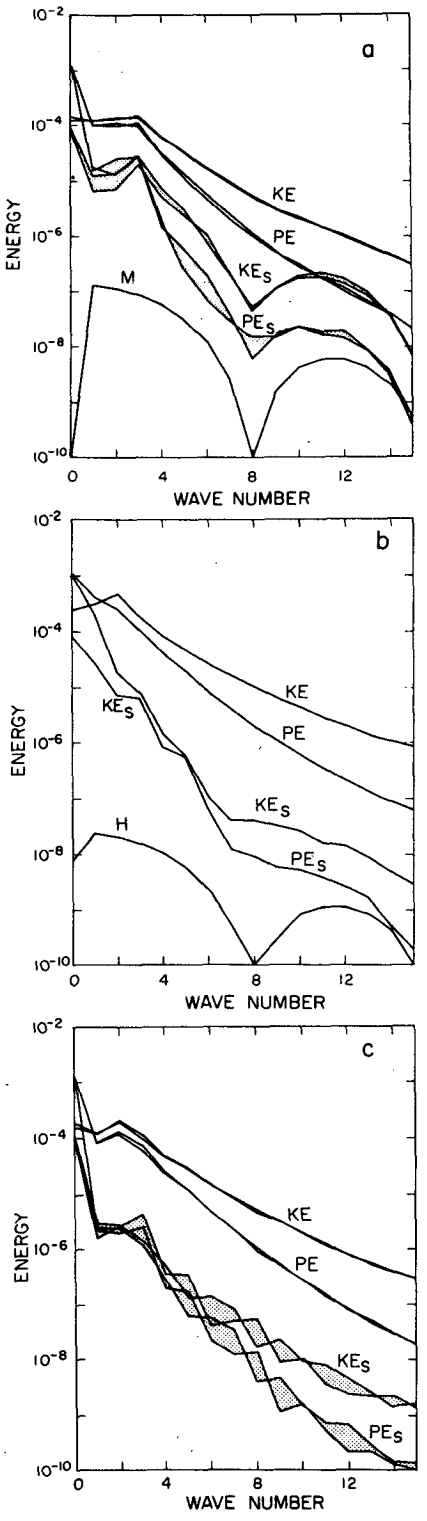

FIG. 6. Kinetic (KE) and potential (PE) energy spectra for (a) M1, (b) H1 and (c) C1. Shaded regions denote integrations from different initial conditions (for M1 and C1 only). Curves without a subscript show the total, time-averaged, energies. A subscript s indicates the energy is that in the stationary field. The curves M and H show the amplitude of the stationary forcing—the mountains (a) and the asymmetric heating in (b). Units are arbitrary.

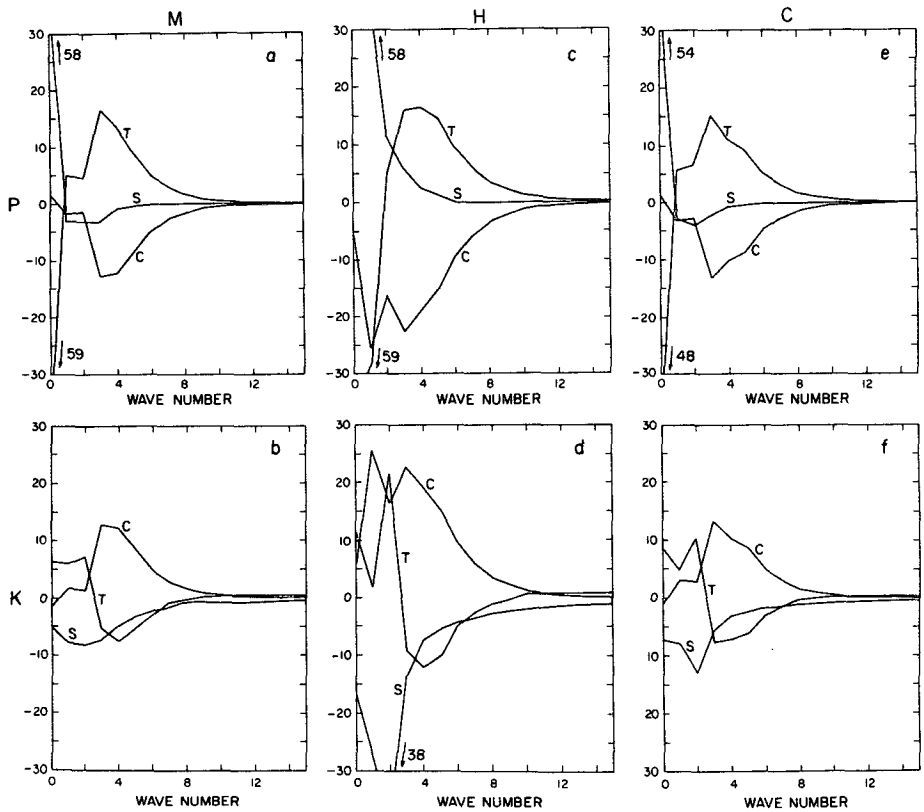

FIG. 7. Total energy budgets for M1 (a and b), H1 (c and d) and C1 (e and f). Units are arbitrary. The upper row is for potential energy, the lower for kinetic. The labels denote: S, diabatic source or frictional sink; C, conversion between potential and kinetic; T, transfer.

Energy enters the (stationary) zonal flow through direct forcing creating zonal available potential energy. Most of it is transferred into transient eddy potential energy, then into transient kinetic where it is dissipated. However, a significant fraction is transferred into stationary eddy potential energy. This is balanced by further transfer to both transient potential energy and to stationary kinetic (see also Holopainen, 1970 and Yao, 1980). Stationary kinetic energy is further converted into transient energy or dissipated. In M1 (and M2) note that the stationary energy budget is dominated by transfers at wavenumber 3. Over 70% of the conversion between zonal and eddy potential energy occurs here, suggesting that wavenumber 3 is linearly resonant with the zonal flow. In H1 and H2 (Figs. 5 and 8) no such potentially resonant structure is noticeable.

Note too that the stationary kinetic energy in M1 and M2 is not maintained by direct orographic forcing (which would be represented by a conversion from zonal kinetic to stationary eddy kinetic energy) but by transfer from potential energy (see also Holopainen, 1970 and Yao, 1980). The balance is maintained partly by direct dissipation and partly by the dissipative effects of the transient eddies. The upscale transfer of energy is accounted for, too, almost entirely in the transients—even at low wavenumbers. The transfer of energy by the purely stationary flow shows no preferred direction.

The major energetic differences between the mountain and heating cases is in the stationary budgets. The direct asymmetric heating now provides the major source of stationary eddy potential energy (Figs. 6 and 8). Nevertheless the eddies themselves are a little stronger, and their kinetic energy is smaller. The reason seems to be an enhanced effect of the transient motion in dissipating the stationary energy. Indeed, increasing the strength of the asymmetric heating (from H2 to H1) succeeds mainly in enhancing this transfer, and increasing the strength of the transient eddies. From Fig. 8 we see the asymmetric heating is relatively more efficient at lower wavenumbers in supplying energy compared with the orographic forcing. [The Jacobian $J(\psi, h)$ provides a wavenumber multiplying the mountain height h, unlike the thermodynamic forcing. Also, the mountain Jacobian is not an energy source; it merely acts to redistribute energy, since $\int \psi J(\psi, h)dx = 0$.] Interestingly, the orographic energy cycle (Fig. 4) resembles qualitatively the winter cycle computed by Holopainen (1970) for

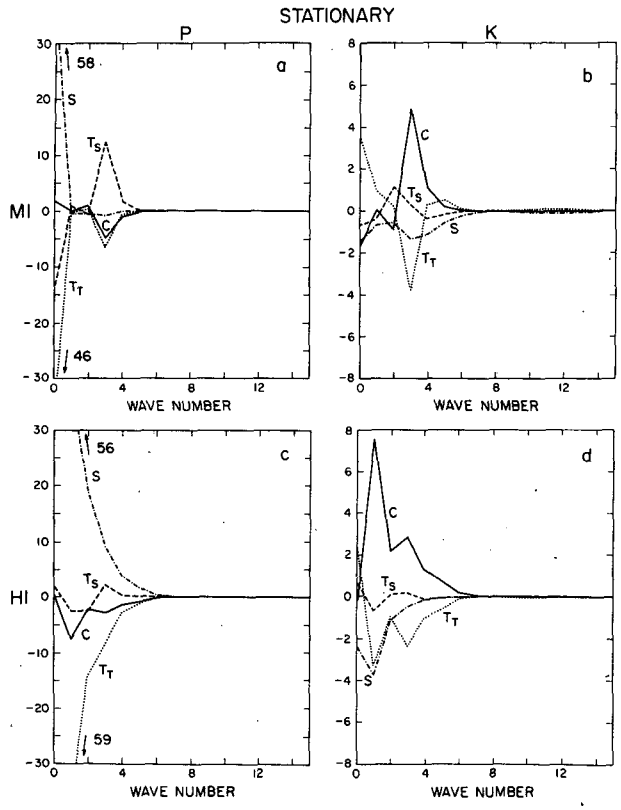

FIG. 8. Energy budgets for the stationary field for M1 [Figs. (a) and (b)] and H1 [Figs. (c) and (d)]. Figs. (a) and (c) show the budget of potential energy, (b) and (d) the kinetic energy budgets. The labels on the curves denote: S, diabatic source or frictional sink; C, conversion between stationary potential and stationary kinetic energy; T_s contribution from/to other stationary modes; T_T contribution to/from transient modes. Note the different scales for the kinetic energy budget. Units are same as Fig. 7.

the real atmosphere whereas the cycle driven thermally (Fig. 5) resembles more closely the summer cycle. This is consistent with orographic (thermal) forcing being more important than thermal (orographic) forcing in winter (summer).

4. Stationary models

In this section we discuss the extent to which the stationary fields of the full model are described by linear or stationary nonlinear models and to what extent the turbulent terms contribute.

a. Time-averaged equations

The time mean asymmetric equations may be written

$$\frac{\partial}{\partial t}[\hat{q}] + \mathbf{G}_\omega[\hat{\psi}] = [\hat{F}], \tag{10}$$

where at the upper level

$$[F] = \lambda^2 A - J([\hat{\psi}_1], [\hat{q}_1]) - [J(\psi_1', q_1')] \tag{11}$$

and at the lower level

$$[F] = -\lambda^2 A - J([\hat{\psi}_3], [\hat{q}_3]) - [J(\psi_3', q_3')] - J([\bar{\psi}_3], \hat{h}_3). \tag{12}$$

A bracket denotes a time average and a prime a deviation therefrom. An overhead bar denotes a zonal average and a carat a deviation therefrom. An integration time of 4 months is more than sufficient to make $\partial[\hat{q}]/\partial t$ negligible. The terms on the rhs in (11) and (12) are the diabatic heating, the fluxes due to the stationary eddies, the turbulent fluxes due to the transient eddies and the linear orographic forcing. Including only the terms in $[\hat{\psi}]$ (i.e., radiative damping, friction and interaction with the zonal flow) and the nonhomogeneous terms in $[F]$ defines the linear model. Including the stationary nonlinear terms in $[F]$ using fields from the full model defines the "stationary nonlinear" model although formally the model is still linear. The transit thermodynamic or vorticity fluxes may also be incorporated in $[F]$. In Eq. (10) $\mathbf{G}_\omega$ is a matrix composed of the frictional terms and terms derived by linearizing the asymmetric equations about the zonal flow. For an inviscid linear model

$$\mathbf{G}_\omega[\hat{\psi}] = J([\bar{\psi}], [\hat{q}]) + J([\hat{\psi}], [\bar{q}]).$$

Setting up the matrix required use of interaction coefficients. The stationary linear solution is then given by $[\hat{\psi}] = \mathbf{G}_\omega^{-1}[\hat{F}]$. Use of the diabatic heating and linear orographic forcing gives the linear asymmetric response which, like a linear Hadley circulation, is not present due to the presence of weak stationary and strong transient fluxes.

b. Physical space comparisons

To examine the asymmetric circulation in more detail we return to the physical space streamfunctions in Figs. 2 and 3. The amplitudes from the linear model are approximately three times too big, although some qualitative features are common. The more noticeable discrepancies, especially for the heating cases, are at the northern and southern edges of the domain. Linear theory appears sensitive to the existence of the critical line (where the zonal wind is zero) and here the linear model is giving very large responses. No such response is evident in the nonlinear integrations. Nor is the linear model a good model of the difference (or anomaly) experiment for the differences H1 − H2 and M1 − M2. That is, the increase of M1 from M2 and especially H1 from H2 is much less than given for linear theory. Comparisons of the kinetic energy for the heating case (Fig. 5) implies that saturation values in the stationary kinetic energy have been reached in that the stationary energy for H2 and H1 is very similar. What does change is the energy in the transient systems.

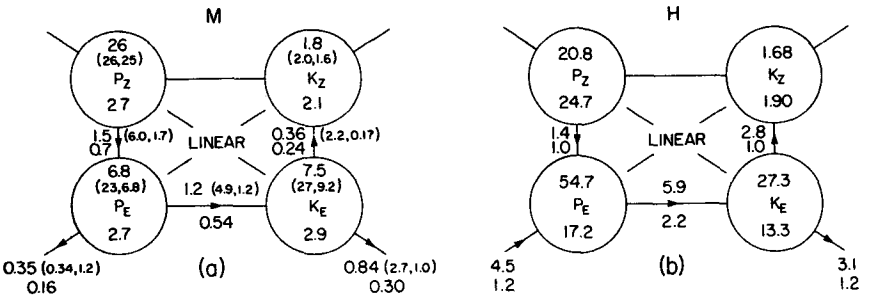

FIG. 9. Energy diagram for linear solutions for mountain (a) and heating (b) cases. In (a), upper numbers are for M1, using the zonally averaged state from a 240-day integration. Figures in brackets use two different 120-day averaged states. Lower figures are for M2. In (b), upper and lower figures are for H1 and H2 respectively. Otherwise, as Figs. 4 and 5.

Quantitative comparisons of the phases of the different fields are given by the correlation coefficient, $\sigma = \int \psi_1\psi_2/(\int \psi_1^2 \int \psi_2^2)^{1/2}$, where the integrals are over the domain. For M1 the correlation between the full and linear models is about 50%. For the difference experiments, M1 − M2, the correlations are similar. For the heating experiment, the correlations are also about 50% but much smaller for the difference. Effectively linear theory seems to work slightly better in this model for the total forcing than it does for anomalous forcings.

c. *Spectral amplitudes and energetics*

The energy cycles for the linear models for the orographic and heating cases are shown in Fig. 9. They are similar to the cycles of the stationary solutions of the full model in that the kinetic energy of the flow is maintained by conversion from potential energy, which in turn is maintained by transfer from the zonal flow (orographic cases) and by direct forcing (heating cases). They differ in that the amplitudes are much higher and the orographic cases display a great sensitivity to the basic state, witnessed by the differing results given by using the zonal state from two different 120 day integrations in M1 and their average (Fig. 9). The first 120 day integration has a zonal state very close to wavenumber-3 resonance. The balance in the stationary kinetic energy is maintained primarily by conversion to zonal kinetic energy, rather than to transients. Again direct orographic forcing is unimportant (i.e., terms directly involving the orography have a small impact on the energetics).

The kinetic energy spectrum for the models is shown in Figs. 10 and 11. In each figure we plot the stationary kinetic energy achieved from an integration of the full model. Additionally we plot the energy from the linear model, this model plus stationary nonlinear forcings (b), and plus transient thermodynamic forcings or plus the transient vorticity forcings (c) and (d). That is, we include the nonlinear terms as nonhomogeneous terms on the right hand side of (10). The models are successive improvements to a basic linear model by the incorporation of additional forcings. If both transient vorticity and thermodynamic fluxes are included, we achieve again the results of the full model.

The abridged models have much higher energies in the stationary fields than the full model. Surprisingly, perhaps, the largest relative discrepancies occur at lower wavenumbers. The linear models are also

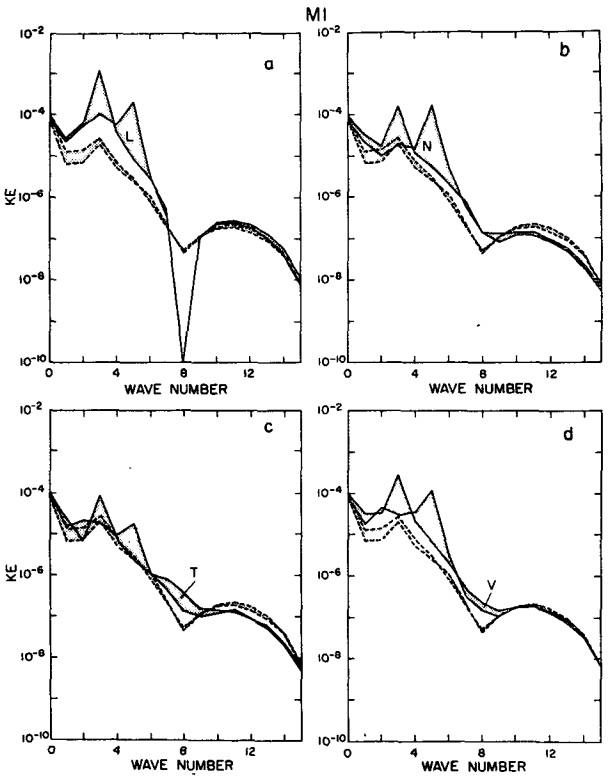

FIG. 10. Comparison of stationary kinetic energy spectra for M1 between full model and various abridgements: (a) Spectra from linear model, (b) stationary nonlinear model spectra, (c) spectra from nonlinear model plus thermodynamic transients, (d) spectra from nonlinear model plus vorticity transients. The spectra from the full model is always shown dashed. Units are arbitrary.

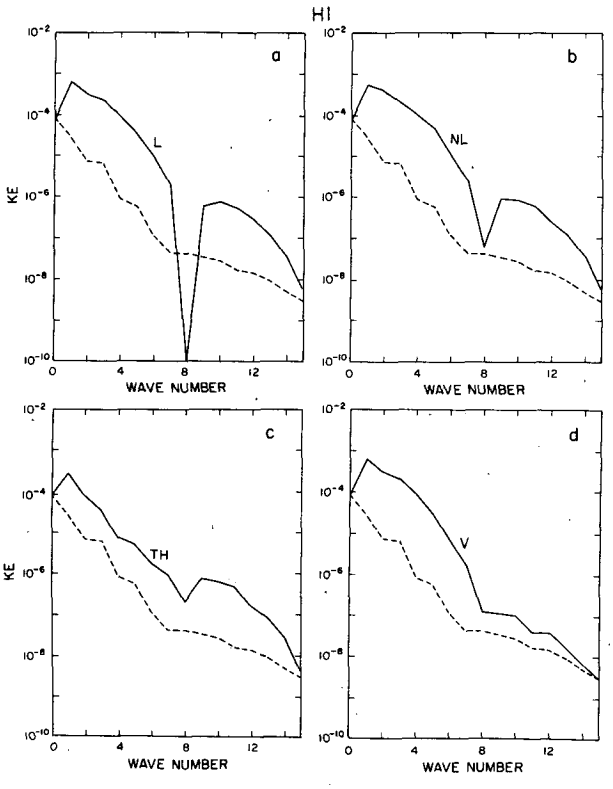

FIG. 11. As in Fig. 10 but for H1.

extremely sensitive to the basic state—note the large differences in M1 in Figs. 9 and 10 for two slightly different zonal winds from the two 120 day integrations. The large amplitude response at wavenumber 3 is due to a simple resonance with the zonal wind. This also occurs in the full model, although its amplitude is greatly reduced by transfer of energy to the transient flow (Fig. 8a and b). In baroclinic flow, the stationary Rossby wave for the first zonal mode at the upper level occurs here near $k_x = 3$. The large response at wavenumber 5 does not seem to be a simple resonance. However, for small surface easterlies resonance can occur near to $k_x^2 = \lambda^2$ (Egger, 1976). (In this model $\lambda \sim$ wavenumber 4.5).

The addition of stationary nonlinear terms, $J([\psi], [q])$, results in a small improvement over the linear model, and the resonant peak at wavenumber 3 is reduced. High sensitivity to the basic state is still displayed. It is primarily the transient terms which are damping the linear response. The thermodynamic transients [the terms of the form $\lambda^2[J(\psi', \tau')]$ are dominant at lower wavenumbers, and the vorticity forcing is dominant at higher wavenumbers. For $k^2 \gg \lambda^2$, inspection of (5) and (6) shows the layers to be effectively decoupled and the transient fluxes of temperature scale out of the problem; for $\lambda^2 \gg k^2$ the temperature field is passively advected by the velocity fields and the fluxes of relative vorticity are small compared with the thermodynamic fluxes in the potential vorticity equation. Qualitatively similar behavior occurs in response to the localized heating, except that the nonlinear stationary forcing has a completely negligible effect. Again transient phenomena are principally responsible for greatly damping the linear response.

The large damping effects of the transient eddies are similar to those found by Youngblut and Sasamori (1980) in a study of the observed circulation, and to the modeling studies of White and Green (1982) and Roads (1981). In these studies the amplitudes of the stationary eddies were greatly reduced by transient thermodynamic fluxes acting on the asymmetric flow. Note also that the stationary energy at all wavenumbers, and not only at resonance, is reduced by the transients.

Of course the beta-plane geometry distorts the nonlinear stationary response, especially in high latitudes where beta is negligible. Saltzman and Sankar-Rao (1963) conclude that stationary nonlinear terms are important in high latitudes in winter. In a spherical model, Ashe (1979) showed that minor modifications occurred when the stationary nonlinear terms were incorporated, although inclusion of a high eddy diffusivity in his study (2.44×10^6 m^2 s^{-1}) makes direct comparison difficult.

d. *Correlations*

In addition to reducing the amplitude of the linear response, the transients affect the phase. A measure of the phase error is given by the correlations C_k between two fields ϕ_k and ψ_k, where

$$C_k = \sum_l \psi_{kl}\phi_{kl} / \left(\sum_l \psi_{kl}^2 \sum_l \phi_{kl}^2\right)^{1/2}.$$

The sums extend over all y wavenumbers l, giving a correlation as a function of zonal wavenumber. The correlations between fields of the full model and fields of the abridged models are shown in Figs. 12 and 13. Note again how little better the stationary nonlinear forcings are over the simple linear model. In all cases, though, linear theory is giving a qualitative picture of both the amplitude and phase of the stationary flow.

5. Instability properties

Having shown that the transient fluxes reduce the amplitude of the stationary flow, and greatly affect the phase, we examine in this section the instability of the climatological flow to small perturbations. Our aim here is to see to what extent the flow variance may be understood in terms of simple instability calculations.

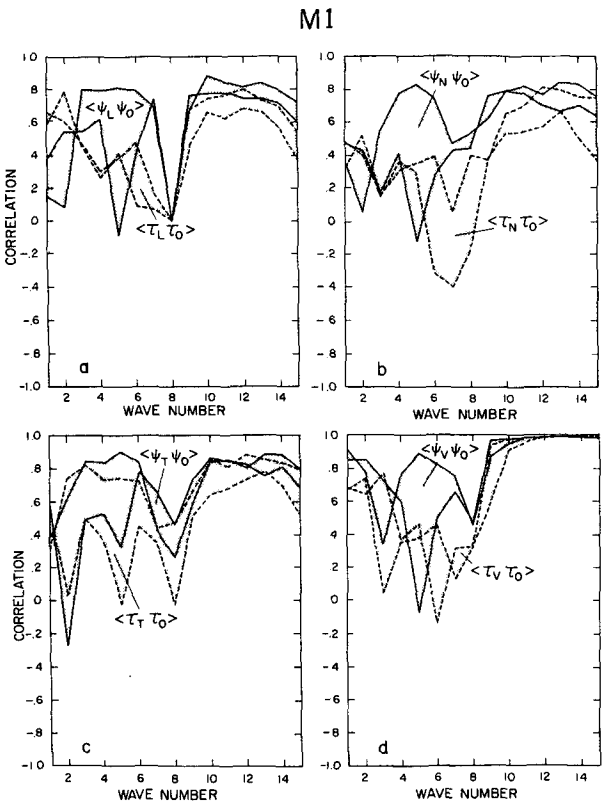

FIG. 12. Correlations for M1, as a function of zonal wavenumber, between thermodynamic and barotropic stationary streamfunctions for the full model and various abridgements: (a) linear model, (b) stationary nonlinear model, (c) nonlinear model plus transient thermodynamic forcings and (d) nonlinear model plus transient vorticity forcings. The solid curves are for ψ, the dashed curves for τ.

a. *Eigenvalue equations*

The time dependent model may be written as

$$H\frac{\partial}{\partial t}\psi' + G\psi' = F'. \tag{13}$$

In (13) **G** is the linear matrix operator derived by linearizing all Jacobians about an equilibrium state—taken here to be the time averaged nonzonal state from the nonlinear time dependent model, and F' is composed of the term $-J(\psi', q')'$. The linear stability properties of the above equation are obtained by setting $F' = 0$. If we assume $\psi' = \tilde{\psi}e^{\sigma t + i\omega t}$, then the eigenvalues and eigenvectors of the matrix equation

$$[\mathbf{H}^{-1}\mathbf{G} + \mathbf{I}(\sigma + i\omega)]\tilde{\psi} = 0$$

where **I** is the identity matrix, give the fundamental frequencies and spatial structure of the time dependent system so long as $J(\psi', q')'$ is negligible. Various simplifications to the above equations are considered. For example, if only the matrix for the asymmetric equations is considered, one zonal wavenumber at a time, the standard baroclinic instability problem of flow linearized around a purely zonal flow results. If in addition the zonal flow as well as the orographic feedback is considered, the wave-mean flow problem considered by Charney and Devore (1979) results. Consideration of the entire system was done first by Lorenz (1972) and most recently by Frederiksen (1983) although without consideration of the orographic feedback.

b. *Instability of the zonally averaged flow*

The baroclinic instability of this standard problem is graphed in Figs. 14 and 15. Note the presence of long-wave and short-wave cutoffs. The long-wave cutoff is due to the effects of beta and especially friction, which damps perturbations with growth rates smaller than a few days. The short-wave cutoff is typically baroclinic—for the canonical problem of a mean shear with no curvature, stability occurs for all $k > \sqrt{2}\lambda$. Phase speeds are also typically baroclinic, and growth rates of about 5 days are found.

The resulting shear for all experiments is well above the critical shear for baroclinic stability, even with friction taken into account. The critical shear is found by systematically reducing the zonal shears obtained in each of the experiments and then calculating the new growth rates. The model shear is

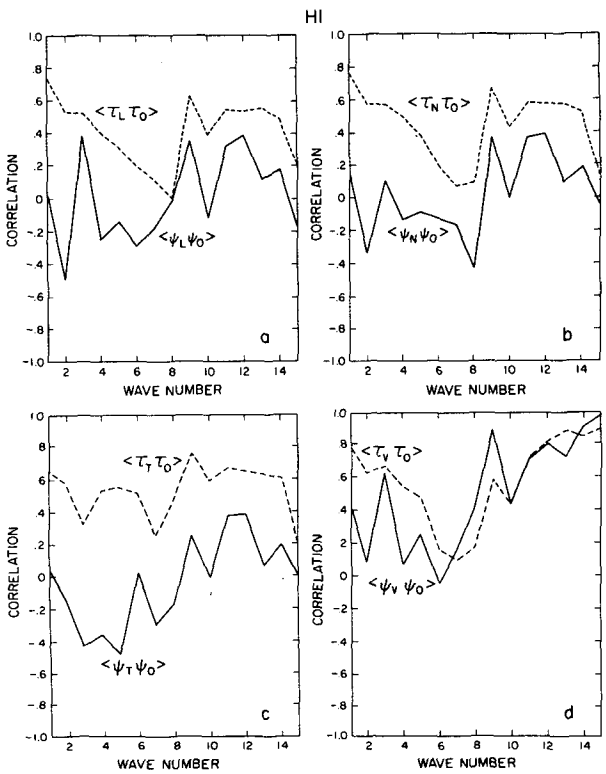

FIG. 13. As in Fig. 12 but for H1.

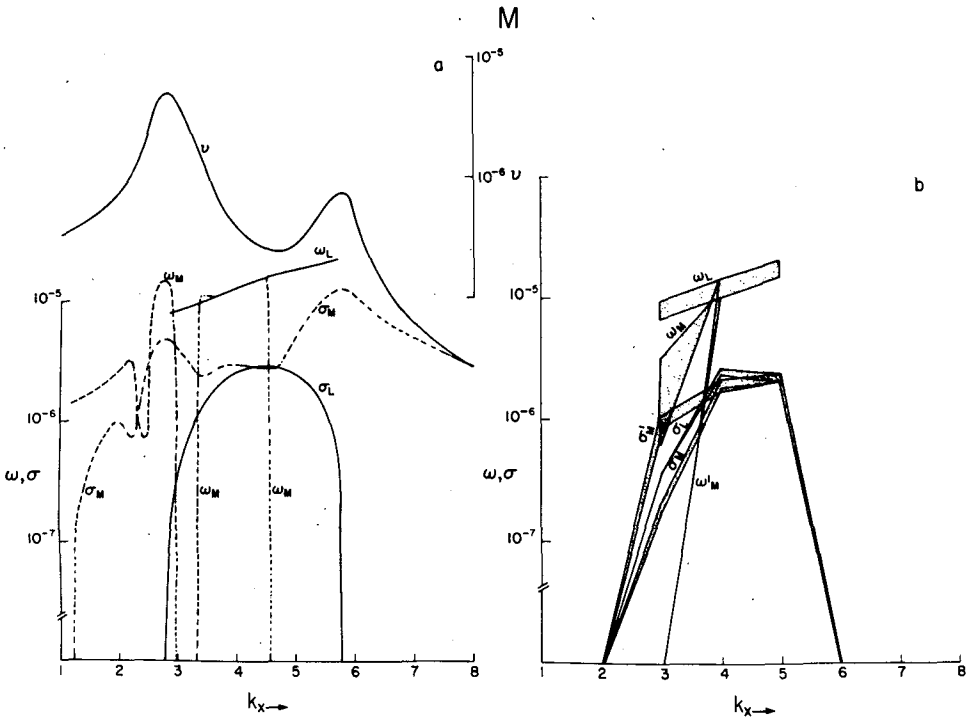

FIG. 14. Instability for case M1 for the standard baroclinic instability problem and for the wave–mean flow instability problem. σ denotes the growth rate and ω the complex frequency of the unstable system in s^{-1}. Subscript l denotes the standard baroclinic instability problem and subscript m the wave–mean flow problem. (a) The response for the idealized problem in which the amplitude of the wave is taken from the linear model. The sum of the squares of the stationary linear amplitudes for the idealized problem is denoted v. (b) The response when the amplitude of the wave is taken from the time averaged model. σ'_m and ω'_m refer here to the wave mean flow instability when the orographic feedback is neglected.

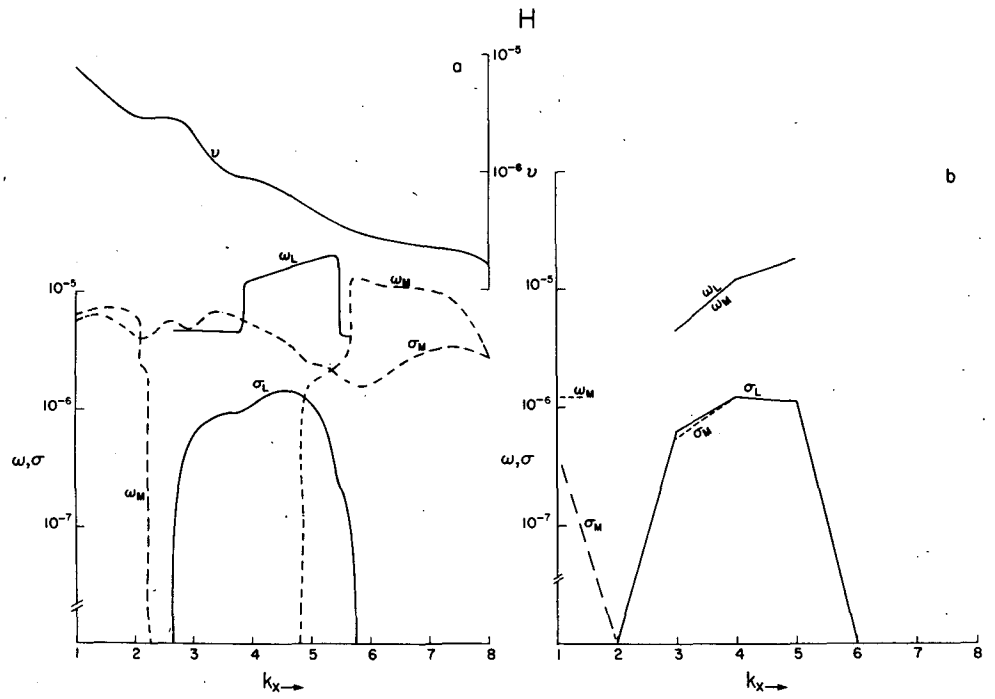

FIG. 15. As in Fig. 14 except for case H1.

approximately double the inviscid critical shear and about 50% larger than the critical shear with friction. In Stone's (1978) study, the atmosphere was shown to lie close to the critical shear of a simplified two-level quasi-geostrophical model on a beta-plane. The fact that our results are not close to criticality implies that either our forcing is much too strong or that baroclinic adjustment is not the dominant mechanism of equilibration. However, if baroclinic adjustment is to work at all, it should work in a two-level, quasi-geostrophic model. A highly supercritical shear seems to be a common feature of a number of quasi-geostrophic simulations. It implies that the baroclinic eddies are not equilibrating through a stabilization of the mean flow (cf. Stone, 1978) but that either transfer to lower and more stable wavenumbers or stochastic equilibration (wherein the forcing due to interaction with other modes destroys the phase correlations necessary for linear instability) is occurring (e.g., Salmon, 1980).

c. *Wave mean flow instability*

The next most simple problem is to examine the stability of a basic state consisting of the mean zonal flow plus that due to the interaction of the zonal flow with the asymmetric forcing of a single wave. It is the simplest problem which explicitly considers the effects of the asymmetric forcing. We performed two sets of calculations. In the first, we take the mean zonal state from the full model, calculate the linear response to orography (for one zonal wavenumber at a time) and then calculate the instability associated with this mean state consisting of a zonal wind and an orographic wave of wavenumber k_x. (We performed these calculations as a continuous function of zonal wavenumber by varying the zonal dimension and using the forcing for the first zonal wavenumber of the discrete model.) The other instability calculation we perform uses the mean state given by the full model integration of both zonal flow and wave motion and uses the corresponding spectral forcing.

The idealized wave–mean flow interaction problem displays greater instability than the linear baroclinic instability problem, especially for low and high wavenumbers (Figs. 14a and 15a). The phase speeds are also changed, generally being slower. We note here that linear resonance is evident, in both orography and heating cases (although more in the former). This is evident in the peak in the linear response just below wavenumber 3 which also is the slowest moving wave. However, this calculation itself is somewhat unrealistic, as can be seen by comparing it with the results from the true mean state (Figs. 14b and 15b). Now the growth rates are very similar to those given by the purely zonal problems, suggesting baroclinic instability is the main contributor at smaller mean state amplitudes. However, the phase speeds are considerably reduced, especially at wavenumber 3. Note too the presence of substantial instability in wavenumber one for the heating case.

The main point we wish to make here is that the idealized wave–mean flow problem is unrealistic as an indicator of the flow stability properties of the climatological flow because the linear amplitude of the waves is generally too high, and the system is too unstable. However, it does suggest why in this model, and perhaps the atmosphere, linear behavior is not observed. That is, the linear state is likely to be highly unstable. Reduction of the orography and heating by ½ tends to also decrease the growth rates by ½ and therefore it is likely that linear theory will work well only for topographic amplitudes an order of magnitude smaller than the ones we have chosen for this study. At high wavenumbers the linear topographic flow is stable. In spite of the flow being highly turbulent here, the stability is presumably ensuring that linear theory performs fairly well.

d. *Three-dimensional instability*

Finally, we give in Table 1 the eigenvalues calculated for the problem of the instability of the complete, time averaged flow. To solve the complete problem requires finding the eigenvalues of a 930^2 matrix, which was beyond our computing resources. We therefore had to truncate the system. In doing the linear solutions it was noticed that it was important to include all meridional modes. Fewer meridional modes were needed only for the higher zonal wavenumbers, where linear theory in any case did a fairly reasonable job for the orographic forcing. The system was therefore truncated at zonal wavenumber 8 but all meridional modes were retained (matrix of order 450).

For the orographic case (M1) three unstable eigenvalues are present, two with large growth rates and fairly rapid oscillations, and a third, more slowly amplifying and oscillating mode. If the orography was removed and the calculation repeated (denoted $M1'$) somewhat different eigenvalues resulted. The most unstable mode has about a 50% higher growth rate and the number of amplifying eigenvalues has increased. Decreasing the meridional truncation wavenumber, $M1''$, gives more or less the same amplitude for the most unstable mode as the less truncated system but more eigenvalues.

The barotropic streamfunction eigenvectors for the orographic case M are given in Fig. 16. Plotted are the time averaged root mean square over one frequency cycle, ignoring the growth and the eigenvector at $t = 0$. The most unstable modes are similar to those given by the standard, linear, baroclinic instability calculations and the variance tends to have little zonal structure, indicating zonally propagating waves. The third mode has zonal structure associated

TABLE 1. Eigenvalues for the three-dimensional instability problem. The real part of the exponent, σ (the growing part), is given first followed by the imaginary part, ω (the oscillating part), in units of s^{-1} (x, y denotes $x \times 10^y$). The e-folding times are given by $1/\sigma$ and periods are given by $2\pi/\omega$. The eigenvalues are ordered by the growth rate. All eigenvalues up to the first stationary mode are given. M1 is the orographic case; M1′ is the orographic case when orography is set to zero and M1″ is the orographic case when the meridional modes are truncated at $k_y = 8$. H1 is the heating case, and C1 is the control case.

	M1		M1′		M1″		H1		C1	
N	σ	ω	σ	ω	σ	ω	σ	ω	σ	ω
1	1.45, −6	1.12, −5	2.12, −6	1.08, −5	1.58, −6	1.17, −5	1.67, −6	2.05, −6	2.24, −6	1.51, −5
2	1.35, −6	1.74, −5	1.69, −6	1.73, −5	1.30, −6	2.18, −5	1.17, −6	1.90, −6	2.03, −6	2.13, −5
3	4.26, −7	1.41, −7	1.65, −6	2.43, −7	1.30, −6	1.57, −5	9.30, −7	2.38, −6	7.92, −7	4.65, −6
4			1.05, −6	3.42, −6	8.61, −7	7.83, −6	8.57, −7	2.09, −7	4.15, −7	4.42, −6
5			5.28, −7	6.43, −6	8.57, −7	2.04, −5	7.87, −7	1.18, −5	3.59, −7	1.06, −5
6			5.22, −7	0.	5.23, −7	1.45, −5	6.96, −7	0.	9.87, −8	1.72, −6
7					5.12, −7	1.09, −5			2.28, −8	0.
8					5.07, −7	1.16, −6				
9					4.88, −7	2.25, −7				
10					3.55, −7	7.61, −6				
11					3.24, −7	2.90, −5				
12					2.51, −7	0.				

with it. The minimum variance is over the mountain and the maximum is away from the mountain. Despite a nonzero phase speed, this mode acts like a standing mode in that its maximum amplitude stays more or less stationary.

Plotted in Fig. 17 are the root mean squares [given by $s = (1/T \int \psi^2 dt)^{1/2}$] for the time integration of the full model. The low-passed fields have been obtained by subjecting the time series of the streamfunction to a Hanning window which filters out periods shorter than five days (a ten day low-pass filter showed little difference). Comparing the eigenfunctions (Fig. 16) with the high- and low-passed variance fields of the numerical model (Fig. 17), one can see a certain amount of resemblance. The fast oscillating modes tend to correspond to the high-passed fields and the more slowly varying mode qualitatively corresponds to the low-passed field.

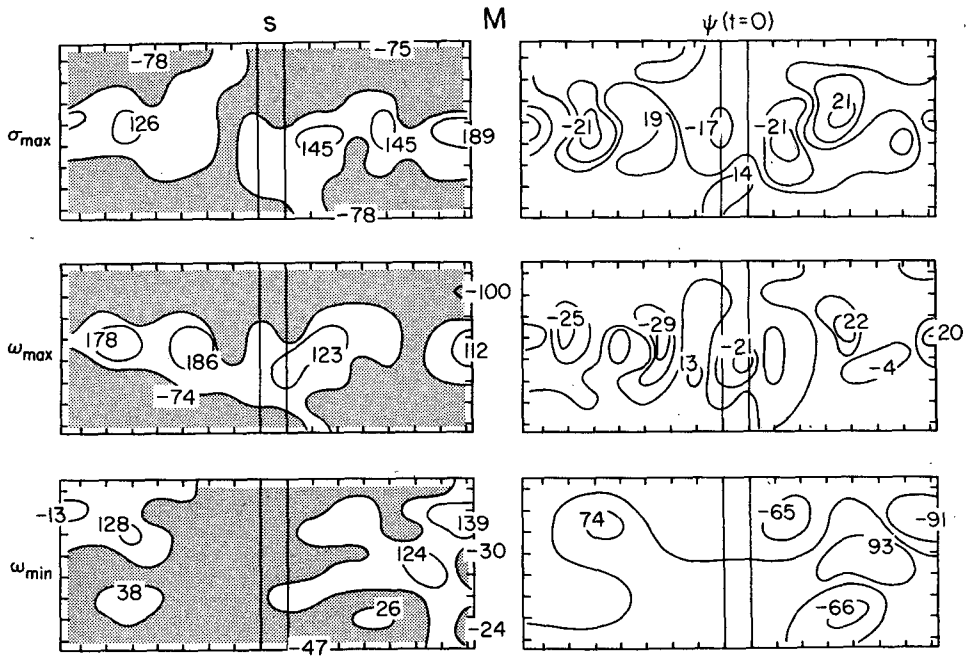

FIG. 16. Eigenvectors for the unstable modes of M1. The most unstable mode is shown first followed by the mode with the largest complex frequency and the mode with the smallest complex frequency. The spatial root-mean-square (rms) (minus the mean value) is given first for each mode followed by the eigenvector present at $t = 0$. The shaded regions have rms values less than the average rms value for the domain. Units are arbitrary.

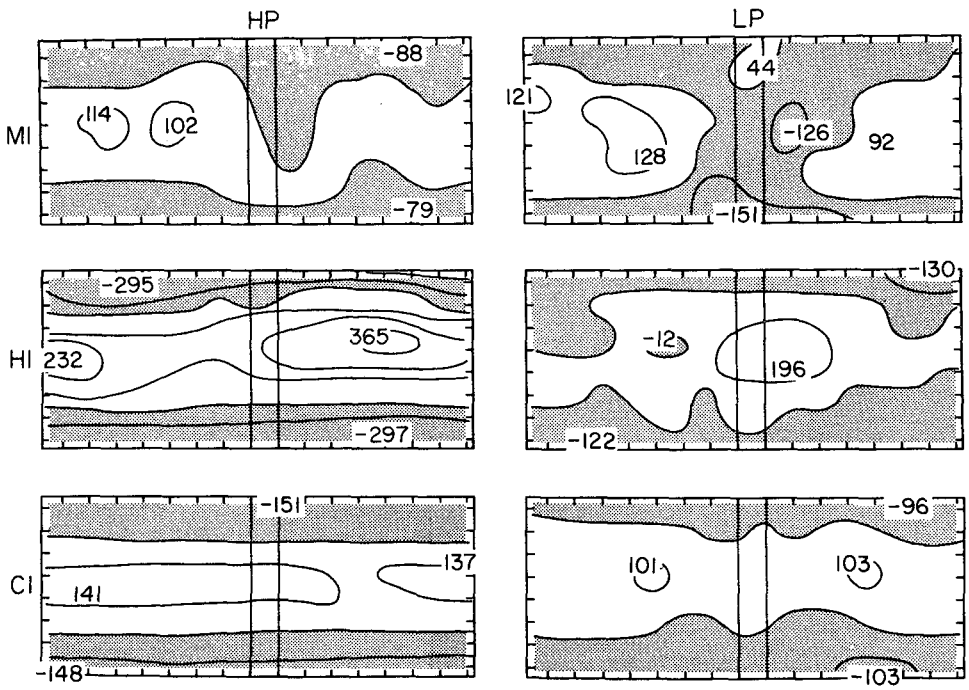

FIG. 17. High- and low-passed rms with the mean value subtracted, from the full model for (a) the orographic case, M1 (b) the heating case, H1 and (c) the control run, C1. Units are arbitrary. Values below zero are shaded.

The heating case was somewhat more difficult to analyze because of the large number of unstable eigenvectors in the system. We show only the fastest growing mode, the fastest moving mode and the slowest moving mode (Fig. 18). The fastest growing mode in this case has zonal structure associated with it and tends to have the maximum variance near the center of the domain similar to the low-passed field

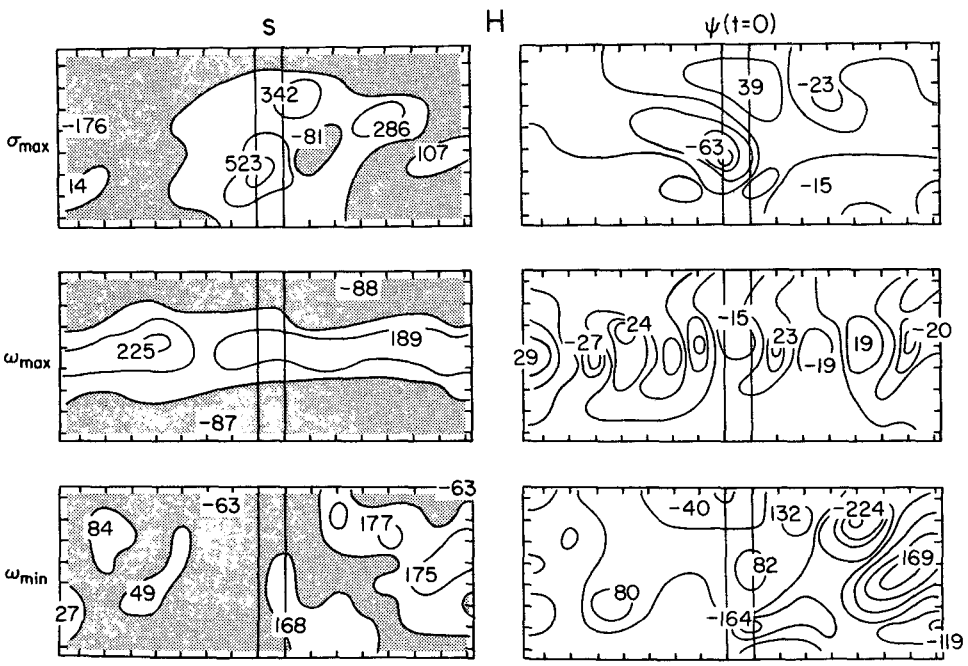

FIG. 18. As in Fig. 16 except for the H1 case.

of the full model. The fastest oscillating mode in this case corresponds most closely to the high-passed variance field of the full model, shown in Fig. 17, with essentially no zonal variation in variance. Note, though, that several eigen-solutions exist which bear little resemblance to the flow, in particular the slowest oscillating mode. This may be due to the choice of a time-averaged basic state which may not be relevant to the instantaneous growth of instabilities.

6. Summary and conclusions

This study has been concerned with the extent to which stationary features of flow over topography are the result of stationary linear dynamics and to what degree nonlinear dynamics, stationary and turbulent, contribute. We integrated a quasi-geostrophic model with idealized topographic forcing for a period of several months and compared the time-averaged results with the results of linear theory. The addition of the stationary nonlinear, thermodynamic and transient vorticity fluxes successively brings the linear model to the full turbulent model.

Before summarizing the results we shall reiterate some of the model limitations. The beta-plane geometry certainly distorts the perceived atmospheric picture seriously in the higher latitudes. Since transient activity is also weak here, we should not expect stationary effects to be so much smaller here. A more serious limitation is the models inability to radiate energy into a stratosphere. If such a radiation were allowed the stationary linear solutions might be weaker and the effects of the transient phenomena smaller, as pointed out by the reviewers.

In spite of these potential limitations the turbulent simulations display atmospheric-like features. The shape of the energy spectra, the direction and magnitude of the energy transfers and the physical space amplitudes are realistic. The energetics of the total flow, transient plus stationary, is typical of quasi-geostrophic turbulence. Most of the upscale transfer of kinetic energy occurs in the transient flow. In all cases transfer of energy between stationary eddy modes has a small contribution. Transfer of energy from the stationary to the transient flow is responsible for reducing the amplitude of the stationary flow, and in particular of the resonant structures which, nevertheless, can still be detected in the turbulent simulations. The energy cycles of the linear solutions are larger but in the same direction as the full solution, except that the main sink of stationary kinetic energy is in the zonal flow, rather than the transients.

The mean zonal state of the model is little altered by the presence of topography. The variation in the zonal state, with and without topography, is no greater than the variation between long-term integrations started from slightly different initial conditions. The zonal wind produced in all cases, in response to a differential heating rate of about 1 K day^{-1}, has about twice the shear needed for instability. Nonlinear turbulent effects rather than a reduction in the mean available potential energy of the zonal state are evidently responsible for producing equilibration.

The asymmetric states show marked differences depending on whether heating or orography is present. The heating case is dominated by the response at wavenumber 1 whereas the orographic case has a Rossby wave train propagating downstream of the mountain with a maximum wavenumber response for $k_z = 3$ corresponding to a simple resonant wavenumber. In the orographic case the linear responses were qualitatively similar except that the linear amplitudes were much too large, especially at the resonant wavenumbers, and somewhat out of phase. The linear heating responses were dominated by the responses near the critical latitudes ($u_3 = 0$). They were very different from the time-averaged turbulent responses.

The topographically forced flow was found highly unstable, although less so at high wavenumbers. The stability properties of the mean field give some indication of the flow variance. In particular, eigenfunctions are present which can be identified with the variance of the high-passed or low-passed time series, perhaps more for the orographic cases. The presence of orography itself is non-negligible and acts to stabilize the flow. In the heating case some eigenfunctions do qualitatively resemble the flow variance, although there is no obvious method of choosing the relevant eigenfunctions.

In summary, we conclude that the transient eddies interact strongly with the asymmetric as well as the zonal flow. Even with the correct zonal state, linear theory overestimates the response of flow over topographic features due to its neglect of the damping effects of the transients which presumably arise from the instability of the flow which would be produced in their absence.

Acknowledgments. The order of authors was determined by the flip of a penny. The research was supported by National Science Foundation Grant ATM82-10160 and by NASA Grant G-NASA-NAG5-236. G. Johnston and V. Roberts text-edited the manuscript and F. Crowe and his group drafted the figures. Useful comments were given by R. C. J. Somerville of Scripps, T. Sasamori of University of Illinois and an anonymous reviewer.

REFERENCES

Alpert, J. C., M. A. Geller and S. K. Avery, 1983: The response of stationary planetary waves to tropospheric forcing. *J. Atmos. Sci.*, **40**, 2467–2483.

Ashe, S., 1979: A nonlinear model for the time-averaged axially asymmetric flow induced by topography and diabatic heating. *J. Atmos. Sci.*, **36**, 109–126.

Boer, G. J., and G. G. Shepherd, 1983: Large scale two-dimensional turbulence in the atmosphere. *J. Atmos. Sci.*, **40**, 164–184.

Charney, J. G., and J. G. Devore, 1979: Multiple flow equilibra in the atmosphere and blocking. *J. Atmos. Sci.*, **36**, 1205–1216.

Egger, J., 1976: The linear response of a hemispheric two-level primitive equation model to forcing by topography. *Mon. Wea. Rev.*, **104**, 351–364.

Frederiksen, J. S., 1978: Instability of planetary waves and zonal flows in two-layer models on a sphere. *Quart. J. Roy. Meteor. Soc.*, **104**, 841–872.

——, 1983: A unified three-dimensional instability theory of the onset of blocking and cyclogenesis. II: Teleconnection patterns. *J. Atmos. Sci.*, **40**, 2593–2609.

Holopainen, E. O., 1970: An observational study of the energy balance of the stationary disturbances in the atmosphere. *Quart. J. Roy. Meteor. Soc.*, **96**, 626–644.

——, L. Rontu and N.-C. Lau, 1982: The effect of large-scale transient eddies on the time-mean flow in the atmosphere. *J. Atmos. Sci.*, **39**, 1872–1984.

Kalnay-Rivas, E., and L.-O. Merkine, 1981: A simple mechanism for blocking. *J. Atmos. Sci.*, **38**, 2077–2091.

Lin, C. A., 1980: Eddy heat fluxes and stability of planetary waves. Part I and Part II. *J. Atmos. Sci.*, **37**, 2353–2380.

Lorenz, E. N., 1972: Barotropic instability of Rossby wave motion. *J. Atmos. Sci.*, **29**, 258–264.

Opsteegh, J. D., and A. D. Vernekar, 1982: A simulation of the January standing wave pattern including the effects of transient eddies. *J. Atmos. Sci.*, **39**, 734–744.

Orszag, S., 1971: Numerical simulation of incompressible flow within simple boundaries. *Stud. Appl. Math.*, **L**, 293–327.

Phillips, T. J., 1982: On the interaction of surface heating anomalies with zonally symmetric and asymmetric atmospheric flows. *J. Atmos. Sci.*, **39**, 1953–1971.

Roads, J. O., 1981: Linear and nonlinear aspects of snow albedo feedbacks in atmospheric models. *J. Geophys. Res.*, **86**, 7411–7424.

Salmon, R. L., 1980: Baroclinic instability and geostrophic turbulence. *Geophys. Astrophys. Fluid Dyn.*, **10**, 25–52.

Saltzman, B., 1968: Surface boundary effects on the general circulation and manoclimate: A review of the theory of the quasi-stationary perturbations in the atmosphere. The causes of climatic change. *Meteor. Monogr.*, No. 30, Boston, Amer. Meteor. Soc., 4–19.

——, and M. Sankar Rao, 1963: A diagnostic study of the mean state of the atmosphere. *J. Atmos. Sci.*, **20**, 438–447.

Sasamori, T., and C. E. Youngblut, 1981: The nonlinear effects of transient and stationary eddies on the winter mean circulation. Part II: The stability of stationary waves. *J. Atmos. Sci.*, **38**, 87–96.

Smagorinsky, J., 1953: The dynamical influence of large-scale heat sources and sinks on the quasi-stationary mean motions of the atmosphere. *Quart. J. Roy. Meteor. Soc.*, **79**, 342–366.

Stone, P. H., 1978: Baroclinic adjustment. *J. Atmos. Sci.*, **35**, 561–571.

Tung, K. K., and R. S. Lindzen, 1980: A theory of stationary long waves. Part II: Resonant Rossby waves in the presence of realistic vertical shears. *J. Atmos. Sci.*, **107**, 735–750.

Vallis, G. K., 1985: On the spectral integration of the quasi-geostrophic equations for doubly-periodic and channel flow. *J. Atmos. Sci.*, **42**, 95–99.

White, A. A., and J. S. A. Green, 1982: A nonlinear atmospheric long wave model incorporating parameterizations of the transient baroclinic waves. *Quart. J. Roy. Meteor. Soc.*, **108**, 55–85.

Yao, M. S., 1980: Maintenance of quasi-stationary waves in a two-level quasi-geostrophic spectral model with topography. *J. Atmos. Sci.*, **37**, 29–43.

Youngblut, C., and T. Sasamori, 1980: The nonlinear effects of transient and stationary eddies on the winter mean circulation. I: Diagnostic analysis. *J. Atmos. Sci.*, **37**, 1944–1957.